doi:10.1038/nature04816

LETTERS

Molecular architecture of axonemal microtubule doublets revealed by cryo-electron tomography

Haixin Sui[1] & Kenneth H. Downing[1]

The axoneme, which forms the core of eukaryotic flagella and cilia, is one of the largest macromolecular machines, with a structure that is largely conserved from protists to mammals[1]. Microtubule doublets are structural components of axonemes that contain a number of proteins besides tubulin, and are usually found in arrays of nine doublets arranged around two singlet microtubules. Coordinated sliding of adjacent doublets, which involves a host of other proteins in the axoneme, produces periodic beating movements of the axoneme. We have obtained a three-dimensional density map of intact microtubule doublets using cryo-electron tomography and image averaging. Our map, with a resolution of about 3 nm, provides insights into locations of particular proteins within the doublets and the structural features of the doublets that define their mechanical properties. We identify likely candidates for several of these non-tubulin components of the doublets. This work offers insight on how tubulin protofilaments and accessory proteins attach together to form the doublets and provides a structural basis for understanding doublet function in axonemes.

Microtubule doublets isolated from sea urchin (*Stronglyocentrotus purpuratus*) sperm were studied by cryo-electron tomography. Groups of up to nine parallel doublets, apparently from a single axoneme, are often found in our frozen–hydrated samples, as shown in Fig. 1 and Supplementary Fig. S2. The protofilaments (PFs) and also the 4 nm tubulin monomer repeat along the PFs are already resolved in the unaveraged tomographic reconstructions (Figs 1 and 2a). As described in Methods, small three-dimensional (3D) volumes along each doublet were extracted from the tomograms and then aligned and averaged. Combining data from nine doublets produced an improved density map, as illustrated in Fig. 2b. Because of the limited angular range over which data are collected the map shows better separation between PF densities in the plane of the specimen than perpendicular to it.

Axonemes contain a number of proteins in addition to tubulin, generally with periodicities that are multiples of the 8 nm tubulin dimer repeat. The longest periodicity detectable in our data from the isolated doublets was 16 nm, so the final map was obtained by filtering the Fourier transform using the layer lines at multiples of 1/(16 nm). Figure 2c is the axial projection of the final density map and shows that the microtubule doublet consists of a complete singlet microtubule, the A-tubule containing 13 PFs, and an incomplete microtubule, the B-tubule, containing ten PFs.

To interpret the structural features of the doublets, we built a pseudo-atomic model of the tubulin component by docking the crystal structure of the α/β tubulin PF (ref. 2) into the 3D density map (Fig. 3a). Unlike singlet microtubules which are circular in cross-section (as in Fig. 1c), the A-tubules show a slight elliptical deformation with an elongation of about 8% in the axoneme's radial dimension. We introduced this distortion in a model of a 13-PF microtubule with a mean radius of 112 Å to construct the A-tubule. The B-tubule was built of 10 straight PFs with a mean radius of 129 Å, which corresponds to the size of a 15-PF microtubule, with a similar distortion in PF positions. For convenience in further discussion, we number PFs as shown in Fig. 3a. To judge the quality of the docking we calculated a density from the atomic model by removing data from its Fourier transform corresponding to the missing data for the experimental map. This calculated density matched the experimental density very well (Fig. 3b), accounting for effects of the anisotropic resolution. The model density accounts for almost all of the experimental density, and the high degree of similarity between the two maps throughout most of the structure makes it straightforward to identify features that represent non-tubulin components of the doublet. A difference map (Figs 3c–f) highlights densities that are clearly not accounted for by tubulin.

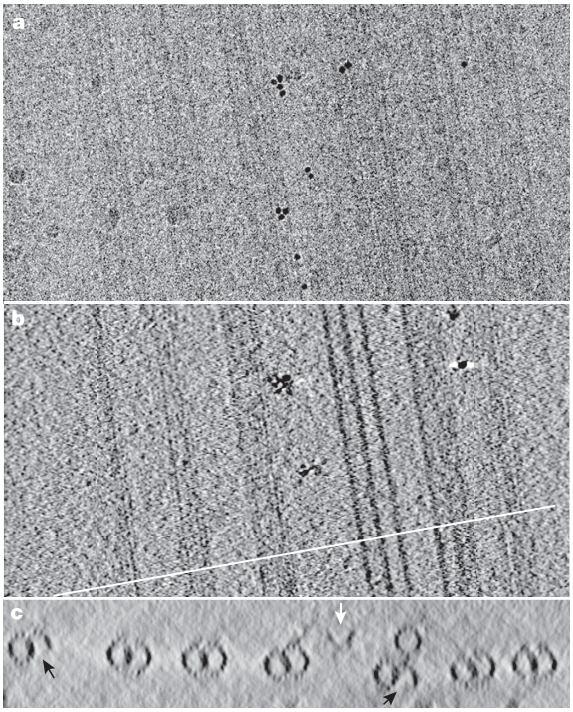

Figure 1 | Electron tomography of microtubule doublets. a, Doublets from a single axoneme are often found parallel to each other, as seen in the zero-tilt image from one tomographic series. **b**, Protofilaments are well resolved in the reconstructions, as shown in a 1-nm-thick section of this tomogram, roughly parallel to the doublets. **c**, A projection of a 26-nm-thick cross-section at the location indicated by the white line in Fig. 1b. The field includes five complete and two broken doublets (black arrows indicate missing PFs) as well as two singlet microtubules, one of which has partially disassembled (white arrow).

[1]Life Sciences Division, Lawrence Berkeley National Laboratory, Berkeley, California 94720, USA.

Towards the outer side of the axoneme, PF B10 is in close contact with A4 and A5, apparently making a tight connection between the A- and B-tubules. In the present model the B10–A5 contact actually contains steric clashes, but the density does not provide sufficient resolution to modify the model reliably and resolve the clashes. Towards the inner side of the axoneme, PF B1 makes the closest approach to A1 but with a gap between the A- and B-tubules.

The region containing PFs A1–A4, referred to as the partition, covers the open part of the B-tubule and separates the hollow space of the two tubules. The PFs of this region can be isolated as a stable ribbon of three adjoining PFs[3–6]. Our map shows how some of the other proteins bound in the partition region help to stabilize this ribbon.

The most distinctive density inside the A-tubule is next to the PFs of the partition, similar to features previously observed in cross-sections of plastic embedded doublets[7]. This density is resolved as a filamentous structure running mainly along PF A3 with projections extending out across several adjacent PFs. Figure 3d is a side view of this region showing three densities running across the partition. Two of these densities extend to PF A1, with an axial repeat of 8 nm, and the other runs across PFs A4 and A5 with a periodicity of 16 nm. These densities form a distinctive bridge-like structure in the longitudinal projection (Fig. 2c) which we term the partition bridge density.

The ribbon formed by the partition contains only a few proteins besides tubulin, including tektins A, B and C[6]. In transmission electron microscope (TEM) studies, a filament which has been shown to contain tektin is frequently seen extending from the end of the ribbon[8–10] (see also Supplementary Fig. S3). Thus we surmise that the only continuous density in the tomogram associated with the ribbon PFs is tektin.

Tektins are predicted to share structural features with intermediate filament proteins (IFPs)[8,10–15], forming heterodimers or homodimers with two globular heads and a coiled-coil structure extending in a tail. Cross-linking studies indicate that tektins A and B form a heterodimer[16]. The present density map is compatible with a number of models for how the tektins are arranged, but a likely interpretation is that the two domains pointing to the right in Fig. 3d correspond to parts of tektin A/B heterodimers, while the density pointing to the left is part of a tektin C homodimer. The continuous filament would then be composed of the head domains, possibly along with parts of the helical domains.

Also on the inside of the A-tubule, there are distinctive densities contacting PFs A7–A13. The density interacting with A10 and A11 protrudes into the lumen of the A-tubule. Another density between PF A12 and A13 projects to the outside of the A-tubule (Fig. 3a–c).

As shown in Fig. 3a, there is a small density projecting out from the doublet in the region of the outer junction between the A- and B-tubules. Because of the positioning of PF B10 in the present model, this feature does not appear in the difference density at the isosurface level used in Fig. 3c. However, if B10 is positioned to produce more realistic contacts with A4 and A5 one could interpret the density as being a small accessory protein that would stabilize the B10–A5 interaction. This protein could bind to both B10 and A5 in the region

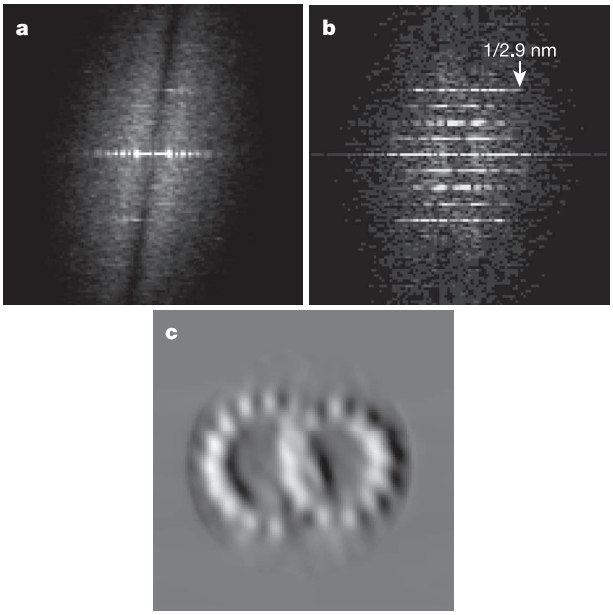

Figure 2 | Results of averaging tomographic data. **a**, Power spectrum of the projection of one doublet from a tomographic reconstruction. The doublet image was computationally straightened before computing the Fourier transform. The layer line at 4 nm is the most prominent. **b**, Power spectrum of the averaged tomogram from nine doublets, showing prominent layer lines at multiples of 1/(16 nm) and extending to a resolution better than 3 nm. **c**, Projection image of the final doublet density map along the longitudinal axis. The orientation was determined by comparison with other work in which doublets have been visualized in the context of the axoneme[29,30]. The view is from the proximal end of the axoneme, and the upward direction corresponds to the outer direction of the axoneme.

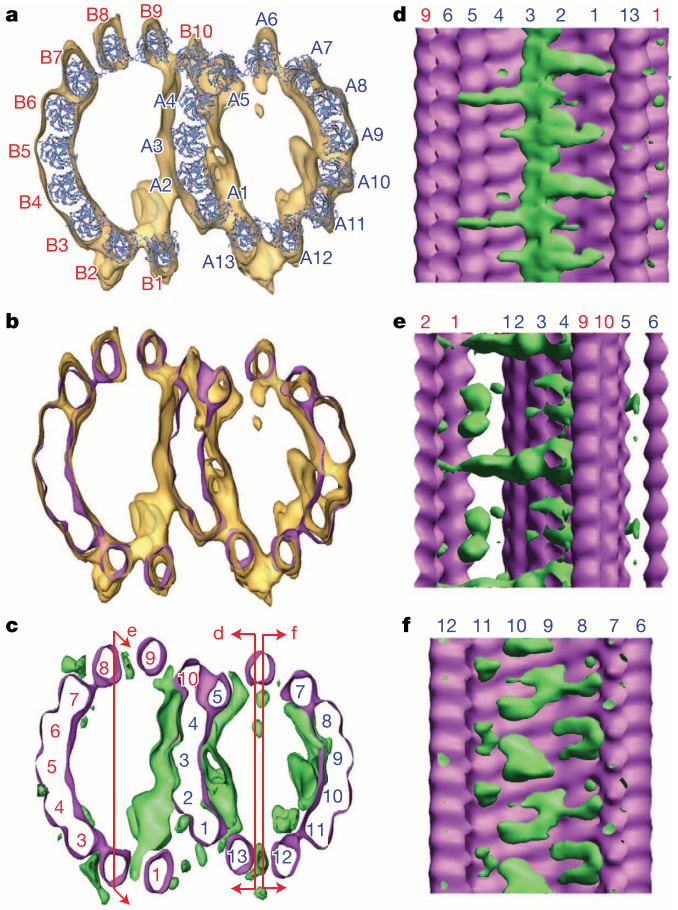

Figure 3 | Interpretation of the 3D density map. **a**, Axial view, seen from the proximal end, of the tomographic reconstruction that was filtered to enhance 16-nm spacings, viewed as an isosurface (yellow). The pseudo-atomic model (backbone only) fitted to the doublet density is shown in blue with labels assigned to the protofilaments. **b**, Projection view of the experimental density in yellow and density calculated from the pseudo-atomic model in purple. **c**, Same views as above with difference map shown in green and model PF density in purple. **d**, **e**, **f**, Side views of the difference map (green) and model density in purple. The orientations are indicated by the red lines in **c**.

occupied by other microtubule-associated proteins (MAPs), but its identity is still unclear.

Our 3D density map reveals a connection every 16 nm between the A and B-tubules towards the inner region (Fig. 3e), which we refer to as the linker density. The linker density connects PF A2 to B1 and extends to PF B2 on one side, with an extension that links PFs A2 and A3 on the outside of the A-tubule. The structure of this linker appears to provide a flexibility that would allow easier twisting of the doublet than if it were a rigid connection. There is another very different density along PF B1 between the linker densities. Some studies had suggested that there might be another PF of the B-tubule in this region, making a direct contact with the A-tubule, but our reconstruction shows that this is not the case.

The most likely candidates for the molecular components of the linker are identified as the polypeptides Sp77 and Sp83 in the isolated ribbons of sperm flagella[6]. Densities with a periodicity of 16 nm are observed at the edge of ribbons[3,7] (see also Supplementary Fig. S3), where immunolabelling studies have identified both Sp77 and Sp83[17], as well as Rib72, a *Chlamydomonas* homologue of Sp77 (refs 18, 19). Immunofluorescence microscopy has also shown that an anti-Sp77 antibody labels the nine doublets but not the central pair singlets, further supporting the hypothesis that Sp77 interacts with both the A- and B-tubules.

The linker density in the tomogram appears to represent a protein significantly larger than 77 kDa and thus probably contains other proteins. Because Sp77 and Sp83 are present in essentially the same amount, it is likely that Sp83 also contributes to the linker protein. Sp83 was found in both doublets and the central pair[17], suggesting that its binding may be more similar to a conventional MAP on the A-tubule rather than directly linking to the B-tubule.

Within the axoneme, there are highly dynamic interactions between doublets arising from the inner and outer dyneins, as well as stable connections formed by nexin[20]. Nexin has been localized in previous electron microscopy studies near the inner side of the doublets[21,22]. In some of our tomograms, where the axonemes are less disrupted, we see a filamentous density that we interpret as nexin connecting PF B2 from one doublet to PFs A9–A11 on the adjacent doublet (Supplementary Fig. S2). Rib72 is also implicated in forming the inter-doublet linkages[19] and may do so via interactions with nexin near PF B2.

Our interpretation of the arrangement of proteins found in the microtubule doublets along with associated proteins described elsewhere in the literature is summarized in Supplementary Fig. S1. The proteins in the partition bridge density, together with the linker density attached to the partition wall outside the A-tubule, clearly play a critical role in stabilizing the PFs near the partition. It appears that they may account for the elliptical distortion of the A-tubule, and they may also provide a substantial increase in resistance to bending of the doublet out of the plane. Other proteins of the A-tubule are located in regions where they could reinforce the tube and help to anchor proteins that bind on the outside. For example, there are distinctive densities inside the regions where the dynein heads are located. The largest feature, on PFs A10–A12, sits inside the attachment region for nexin and the dynein regulatory complex with which it is associated[23–26]. The density we observe between PFs 12 and 13 is at the point where the radial spokes meet the doublets and may be part of their attachment. These external proteins have larger periodicities than the features we see in the doublets, and further work will be required to fully understand the significance of their interactions. The proteins that bind inside the A-tubule do so in a way very different from other MAPs, with the possible exception of tau[27], linking adjacent PFs in ways that seem to supplement the normal inter-PF interactions.

The configuration of the proteins that comprise the microtubule doublet appears to be designed to stabilize and maintain the protofilament architecture of the doublet as it undergoes the stresses involved in axoneme motion and also to favour bending in the direction that corresponds to twisting of the axoneme. Our structure of the microtubule doublet provides insights into several novel tubulin–protein interactions and the functions doublets perform in axonemes, and will serve as a greatly improved basis for quantitative modelling of mechanical properties.

METHODS

Sperm flagella axonemes were prepared from sea urchin following the protocol in ref. 28. For the PF ribbon samples, material was treated with 0.7% Sarkosyl in 10 mM Tris-HCl (pH 7.8) at 4 °C for about 6 h and then centrifuged at 100,000 *g* for 30 min. The pellet was collected and resuspended in the above Tris buffer without Sarkosyl.

The concentrated doublet sample was resuspended in water containing 5 or 10 nm colloidal gold particles (Ted Pella), and applied to a grid covered with a glow-discharged holey carbon film. Grids were blotted, plunge-frozen in liquid ethane and transferred under liquid nitrogen to the cryo-tilt holder of a JEOL 3100FEF electron microscope. The microscope, operating at 300 kV, was equipped with an Omega energy filter set to a slit width of 25 eV. Microtubule doublets nearly parallel to the tilt axis were selected for data collection. Tomographic data were collected under low-dose conditions with accumulated dose of about 6,500 electrons per nm^2. Single-axis tilt series, including 33–46 images with a tilt increment of 3–4°, were recorded at a defocus of 3.5 to 5 μm on a 2,048 × 2,048 charge-coupled device camera (Gatan). The final pixel size of the images was about 0.53 nm.

Three-dimensional segment volumes along each doublet microtubule were extracted from the tomographic reconstructions. The volumes were aligned and averaged as described in Supplementary Information.

For modelling, the atom coordinates of the PF models for the A- and B-tubules were separately calculated as described in the text using the backbone atoms from the tubulin crystal structure, Protein Data Bank PDB ID 1JFF, and manually shifted into the density as a whole.

Received 6 February; accepted 21 April 2006.
Published online 31 May 2006.

1. Kohl, L. & Bastin, P. The flagellum of trypanosomes. *Int. Rev. Cytol.* **244,** 227–285 (2005).
2. Nogales, E., Wolf, S. G. & Downing, K. H. Structure of the αβ tubulin dimer by electron crystallography. *Nature* **391,** 199–203 (1998).
3. Witman, G. B., Carlson, K., Berliner, J. & Rosenbaum, J. L. *Chlamydomonas* flagella. I. Isolation and electrophoretic analysis of microtubules, matrix, membranes, and mastigonemes. *J. Cell Biol.* **54,** 507–539 (1972).
4. Witman, G. B., Carlson, K. & Rosenbaum, J. L. *Chlamydomonas* flagella. II. The distribution of tubulins 1 and 2 in the outer doublet microtubules. *J. Cell Biol.* **54,** 540–555 (1972).
5. Meza, I., Huang, B. & Bryan, J. Chemical heterogeneity of protofilaments forming the outer doublets from sea urchin flagella. *Exp. Cell Res.* **74,** 535–540 (1972).
6. Linck, R. W. & Norrander, J. M. Protofilament ribbon compartments of ciliary and flagellar microtubules. *Protist* **154,** 299–311 (2003).
7. Linck, R. W. Flagellar doublet microtubules: fractionation of minor components and α-tubulin from specific regions of the A-tubule. *J. Cell Sci.* **20,** 405–439 (1976).
8. Linck, R. W. & Langevin, G. L. Structure and chemical composition of insoluble filamentous components of sperm flagellar microtubules. *J. Cell Sci.* **58,** 1–22 (1982).
9. Linck, R. W., Amos, L. A. & Amos, W. B. Localization of tektin filaments in microtubules of sea urchin sperm flagella by immunoelectron microscopy. *J. Cell Biol.* **100,** 126–135 (1985).
10. Linck, R. W. & Stephens, R. E. Biochemical characterization of tektins from sperm flagellar doublet microtubules. *J. Cell Biol.* **104,** 1069–1075 (1987).
11. Chang, X. J. & Piperno, G. Cross-reactivity of antibodies specific for flagellar tektin and intermediate filament subunits. *J. Cell Biol.* **104,** 1563–1568 (1987).
12. Linck, R. W., Albertini, D. F., Kenney, D. M. & Langevin, G. L. Tektin filaments: chemically unique filaments of sperm flagellar microtubules. *Cell Motility Suppl.* **1,** 127–132 (1982).
13. Chen, R., Perrone, C. A., Amos, L. A. & Linck, R. W. Tektin B1 from ciliary microtubules: primary structure as deduced from the cDNA sequence and comparison with tektin A1. *J. Cell Sci.* **106,** 909–918 (1993).
14. Norrander, J. M., Amos, L. A. & Linck, R. W. Primary structure of tektin A1: comparison with intermediate-filament proteins and a model for its association with tubulin. *Proc. Natl Acad. Sci. USA* **89,** 8567–8571 (1992).
15. Steffen, W. & Linck, R. W. Relationship between tektins and intermediate filament proteins: an immunological study. *Cell Motil. Cytoskel.* **14,** 359–371 (1989).
16. Pirner, M. A. & Linck, R. W. Tektins are heterodimeric polymers in flagellar microtubules with axial periodicities matching the tubulin lattice. *J. Biol. Chem.* **269,** 31800–31806 (1994).

17. Hinchcliffe, E. H. & Linck, R. W. Two proteins isolated from sea urchin sperm flagella: structural components common to the stable microtubules of axonemes and centrioles. *J. Cell Sci.* **111,** 585–595 (1998).
18. Patel-King, R. S., Benashski, S. E. & King, S. M. A bipartite Ca2+-regulated nucleoside-diphosphate kinase system within the *Chlamydomonas* flagellum. The regulatory subunit p72. *J. Biol. Chem.* **277,** 34271–34279 (2002).
19. Ikeda, K. *et al.* Rib72, a conserved protein associated with the ribbon compartment of flagellar A-microtubules and potentially involved in the linkage between outer doublet microtubules. *J. Biol. Chem.* **278,** 7725–7734 (2003).
20. Lindemann, C. B. Testing the geometric clutch hypothesis. *Biol. Cell.* **96,** 681–690 (2004).
21. Bozkurt, H. H. & Woolley, D. M. Morphology of nexin links in relation to interdoublet sliding in the sperm flagellum. *Cell Motil. Cytoskel.* **24,** 109–118 (1993).
22. Woolley, D. M. Studies on the eel sperm flagellum. I. The structure of the inner dynein arm complex. *J. Cell Sci.* **110,** 85–94 (1997).
23. Huang, B., Ramanis, Z. & Luck, D. J. Suppressor mutations in *Chlamydomonas* reveal a regulatory mechanism for flagellar function. *Cell* **28,** 115–124 (1982).
24. Gardner, L. C., O'Toole, E., Perrone, C. A., Giddings, T. & Porter, M. E. Components of a "dynein regulatory complex" are located at the junction between the radial spokes and the dynein arms in *Chlamydomonas* flagella. *J. Cell Biol.* **127,** 1311–1325 (1994).
25. Piperno, G., Mead, K., LeDizet, M. & Moscatelli, A. Mutations in the "dynein regulatory complex" alter the ATP-insensitive binding sites for inner arm dyneins in *Chlamydomonas* axonemes. *J. Cell Biol.* **125,** 1109–1117 (1994).
26. Piperno, G., Mead, K. & Shestak, W. The inner dynein arms I2 interact with a "dynein regulatory complex" in *Chlamydomonas* flagella. *J. Cell Biol.* **118,** 1455–1463 (1992).
27. Kar, S., Fan, J., Smith, M. J., Goedert, M. & Amos, L. A. Repeat motifs of tau bind to the insides of microtubules in the absence of taxol. *EMBO J.* **22,** 70–77 (2003).
28. Waterman-Storer, C. M. in *Current Protocols in Cell Biology* (eds Bonifacino, J. S., Dasso, M., Harford, J. B., Lippincott-Schwartz, J. & Yamada, K. M.) 13.1.6–13.1.7 (John Wiley, New York, 1998).
29. Hoops, H. J. & Witman, G. B. Outer doublet heterogeneity reveals structural polarity related to beat direction in *Chlamydomonas* flagella. *J. Cell Biol.* **97,** 902–908 (1983).
30. Mastronarde, D. N., O'Toole, E. T., McDonald, K. L., McIntosh, J. R. & Porter, M. E. Arrangement of inner dynein arms in wild-type and mutant flagella of *Chlamydomonas*. *J. Cell Biol.* **118,** 1145–1162 (1992).

Supplementary Information is linked to the online version of the paper at www.nature.com/nature.

Acknowledgements We thank A. Killilea for sea urchin collection, K. Gull for discussions on protofilament numbering, H. Li, B. Rockel and D. Typke for discussions and help with image processing, B. Heymann and C. Yang for discussions and help with BSOFT library usage, and R. Glaeser and M. Auer for suggestions and encouragement. This work is supported by NIH grants and by the US Department of Energy.

Author Information Reprints and permissions information is available at npg.nature.com/reprintsandpermissions. The authors declare no competing financial interests. Correspondence and requests for materials should be addressed to K.H.D. (khdowning@lbl.gov).